Fluorescence resonance energy transfer within Eu(III)-doped ZnO quantum dots embedded in SiO_2 matrix

Jue-Fei Zhou[a], Bo-Long Li[a], Guo-Dong Li[b], Huan-Ming Xiong[a,*]

[a] *Department of Chemistry, Fudan University, Shanghai 200433, P. R. China*
[b] *State Key Laboratory of Inorganic Synthesis and Preparative Chemistry, College of Chemistry, Jilin University, Changchun 130012, P. R. China*

[*] *Author for correspondence: Huan-Ming Xiong, email: hmxiong@fudan.edu.cn*
Received 23 Jul 2014; Accepted 01 Sep 2014; Available Online 01 Sep 2014

Abstract

Eu^{3+} ions doped ZnO quantum dots (QDs) with red fluorescence are prepared successfully in the SiO_2 matrix and their compositions and structures are investigated by infrared spectra, energy-dispersive X-ray spectroscopy, X-ray photoelectron spectroscopy, transmission electron microscope and scanning electron microscope. The SiO_2 matrix protects the ZnO QDs from aggregation and maintains the luminescent properties of ZnO QDs. After careful optical characterizations, a reasonable mechanism is suggested to illustrate the fluorescence emission and the energy transfer processes within the Eu^{3+} ions doped ZnO QDs.

Keywords: ZnO; Eu; Doping; Energy transfer; Photoluminescence

1. Introduction

In the past decade, ZnO QDs have shown potential applications in biological fluorescent probes [1-4] and many photo-electronic devices [5-8] due to their special photoluminescent properties, low cost, green production and safety toward biological systems. However, ZnO QDs have several limitations in their photoluminescence (PL), such as dependence on ultraviolet excitation (300 ~ 360 nm) which is harmful to biological tissues and emission wavelength limited within 450~580 nm region which is not benefit for imaging animals *in vivo*. In order to overcome the above shortcomings, many rare earth elements, such as Eu [9-16], Gd [17], Er [18], Nb [19] and La [20], have been doped into ZnO nanocrystals to improve the optical properties. Among them, Eu^{3+} doped ZnO nanoparticles were investigated most intensively because Eu^{3+} ions exhibit the typical red fluorescence that ZnO QDs lack and the blue laser with wavelength of 400~450 nm is able to excite Eu^{3+} ions fluorescence. However, due to the charge imbalance, radius mismatch and "self-purification" process [21-26], the rare earth dopants tend to be excluded out of the ZnO host thermodynamically and thus it is difficult to dope Eu^{3+} ions into ZnO lattice actually. Furthermore, the doping procedure always needs high temperature treatment which renders heavy agglomeration of ZnO QDs and quenches the ZnO visible fluorescence [9-11, 14-16].

In the present research, Eu^{3+} doped ZnO QDs with red fluorescence were prepared successfully in silica matrix after calcination at 650 ^oC. Due to SiO_2 protection, the visible fluorescence from ZnO defects was remained. After detailed characterizations on the product structures and properties, the effective energy transfer between ZnO and Eu^{3+} was verified, which illustrated the mechanism for the improved red fluorescence of the anneal products. Since the ZnO-Eu@SiO_2 core-shell nanoparticles were stable in water, they were promising in labeling cells. And their red fluorescence could avoid the overlap with the auto-fluorescence of the cells and present more clear images under the laser confocal microscope.

2. Experimental Details

2.1. Chemicals

Methacrylic acid (MAA), zinc oxide (ZnO), absolute ethanol (CMOS grade), europium oxide (Eu_2O_3), ethyl acetate, lithium hydroxide monohydrate ($LiOH•H_2O$), tetraethoxysilane (TEOS, A.R.), Ammonia (25 wt.% aqueous solution) and nitric acid (65 wt.% aqueous solution) were all purchased from Sinopharm Chemical Reagent Co., Ltd.

2.2. Synthesis

MAA was mixed with deionized water by a volume ratio of MAA/H_2O = 1/4 and then reacted with appropriate amount of ZnO powder at 60 ^oC for about 1 h to get zinc methacrylate ($Zn(MAA)_2$). The unreacted ZnO powder was removed by filtration. Such zinc methacrylate aqueous solution was concentrated and dried by rotary evaporation at 70 ^oC and then dehydrated in a vacuum oven at 80 ^oC for 24 h. $Eu(MAA)_3$ was prepared in the same way. ZnO nanoparticles were synthesized through a sol–gel reaction between $Zn(MAA)_2$ and LiOH with the molar ratio [LiOH]/[Zn] = 1.6 in absolute ethanol. For Eu-doped ZnO QDs, different molar percentages of $Eu(MAA)_3$ were added into the reaction system (m% = [Eu]/([Eu]+[Zn]), and m= 0, 5, 10, 20, 50). The solution was concentrated in a rotating evaporator at 40 °C until some white gel emerged, then followed by adding excess ethyl acetate. The precipitated ZnO-Eu(m%) QDs were separated by centrifugation and then dissolved in 100 mL of absolute ethanol.

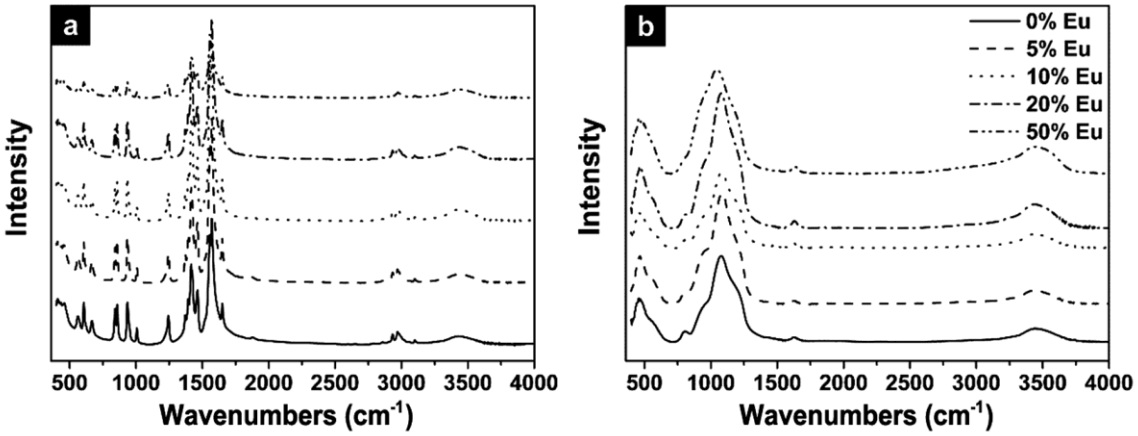

Figure 1. FTIR spectra of (a) ZnO-Eu(m%) QDs and (b) ZnO-Eu(m%)@SiO_2 annealed at 650 ^oC.

20 mL of ZnO-Eu(m%) ethanol colloid was diluted to 100 mL, then mixed with a solution containing 500 μL of TEOS and 25 mL of ethanol. Afterwards, a solution containing 400 μL of ammonia (25 wt.%), 3 mL of H_2O and 25 mL of ethanol was added into the reaction system. After stirring at room temperature for 24 h, the precipitates were centrifuged and washed with absolute ethanol for 3 times, followed by drying at 60 ^oC. The powder was introduced to the middle of a quartz tube in a horizontal furnace and heated at 650 ^oC for 3 h.

2.3. Characterizations

For PL measurements, a small amount of the as-prepared powder was redispersed in water and sonicated by a titanium horn with a power of 1500 W for 10 min on a Sonics VCX 1500 sonicator. PL spectra were recorded by a Horiba Fluoromax-4 fluorescence spectrophotometer. The sample morphologies were inspected using a JEM-2100 Transmission Electron Microscope (TEM) operating at 200 kV and a FE-SEM-4800-1 Scanning Electron Microscope. Element analyses were carried out on an Energy-dispersive X-ray spectroscopy (EDS) equipped on the TEM. To determine the actual content of Eu in each sample, the powder was dissolved in an aqueous solution of HNO_3 via microwave digestion and tested with a Rayleigh WFX-110 inductively coupled plasma (ICP) mass spectrometer. X-ray photoelectron spectroscopy (XPS) analyses were carried out using a Perkin-Elmer PHI5000c. Infrared measurements were conducted on a Nicolet Impact 360 FTIR spectrometer. The lifetimes of the fluorescence were tested on a FLSP 920 combined fluorescence lifetime & steady state spectrometer.

3. Results and Discussion

The incorporation of trivalent rare earth ions into ZnO nanocrystal lattices is a difficult task because of the charge imbalance and the ionic radius mismatching [27] between Zn(II) ions and Eu(III) ions. Moreover, the rare earth ions tend to aggregate on ZnO grain surfaces according to the "self-purification theory" [21, 26, 28]. As a result, many rare earth ions doped ZnO in literature are actually ZnO nanoparticles with the adsorbed rare earth ions on the surfaces. In those cases, the so-called "doped" ZnO exhibits unstable PL features, especially in water, and low efficiencies of energy transfer from the host to the guest. In order to dope Eu^{3+} into ZnO lattice, high temperature diffusion in solid state is necessary. A solid protection shell, which should be transparent optically, is also required for avoiding ZnO QDs agglomeration and growth, because ZnO visible fluorescence is highly dependent on the nanoparticle size and crystallinity. In the FTIR spectra of the as-prepared ZnO-Eu(m%) samples (Figure 1a), the strong absorption bands of organic groups are ascribed to the MAA ligands on the ZnO surface, which stabilizes ZnO QDs for the subsequent silica coating. The SiO_2 matrix protects ZnO QDs during high temperature calcination. After the organic molecules are burnt away, only three absorption bands are observed in Figure 1b, which are ascribed to the Zn-O vibrations (~460 cm^{-1}), Si-O-Si symmetrical stretching (~1100 cm^{-1}) and O-H absorption (~3400 cm^{-1}). These IR absorption bands do not change significantly when the Eu content varies, indicating that Eu doping does not affect the surface states of ZnO nanoparticles.

After calcination at 650 ^oC, the ZnO-Eu(5%)@SiO_2 kept the uniform spherical morphology but stacked with each other (Figure 2a), while the possible impurities like the uncoated ZnO or Eu_2O_3 with non-spherical shape are not seen in the SEM image. In the HRTEM images (Figure 2b-d), the ZnO QDs with their average diameters of 3.1 nm, 2.9 nm, 2.5 nm (m = 0, 5, 20) are homogeneously dispersed in the SiO_2 matrix, and the insets confirm the narrow size distribution of ZnO QDs. Obviously, the SiO_2 matrix plays a key role in preventing the QDs from aggregation during calcination. It is known that ZnO nanoparticles have typical interplanar spacings of 0.245, 0.261 and 0.279 nm, corresponding to the (101), (002) and (100) facets of the wurtzite structure. With respect to the (002) facet, the ZnO spacing increases from 0.261 to 0.265 and 0.267 nm respectively in the Eu^{3+} doped samples (Figure 2c and d). Since Eu^{3+} ion has a larger radius (0.95 Å) than Zn^{2+} ion (0.74 Å), incorporation of Eu^{3+} ions will expand the ZnO lattice spacing undoubtedly. The inset selected area electron diffraction (SAED) and fast Fourier transformation (FFT) patterns also confirm that the increase of m value renders the ZnO lattice spacing expansion. In Figure 2 c and d, a new lattice spacing of about 0.328 nm is also observed, which corresponds to the (222) facet of cubic Eu_2O_3. The self-purification theory [21-26] points out that the solubility of Eu^{3+} in the ZnO lattice is limited, so that the excess Eu^{3+} will be excluded out of ZnO to form Eu_2O_3 nanoparticles. In fact, with the increment of m value, more and more Eu_2O_3 nanoparticles are produced in the SiO_2 matrix. As

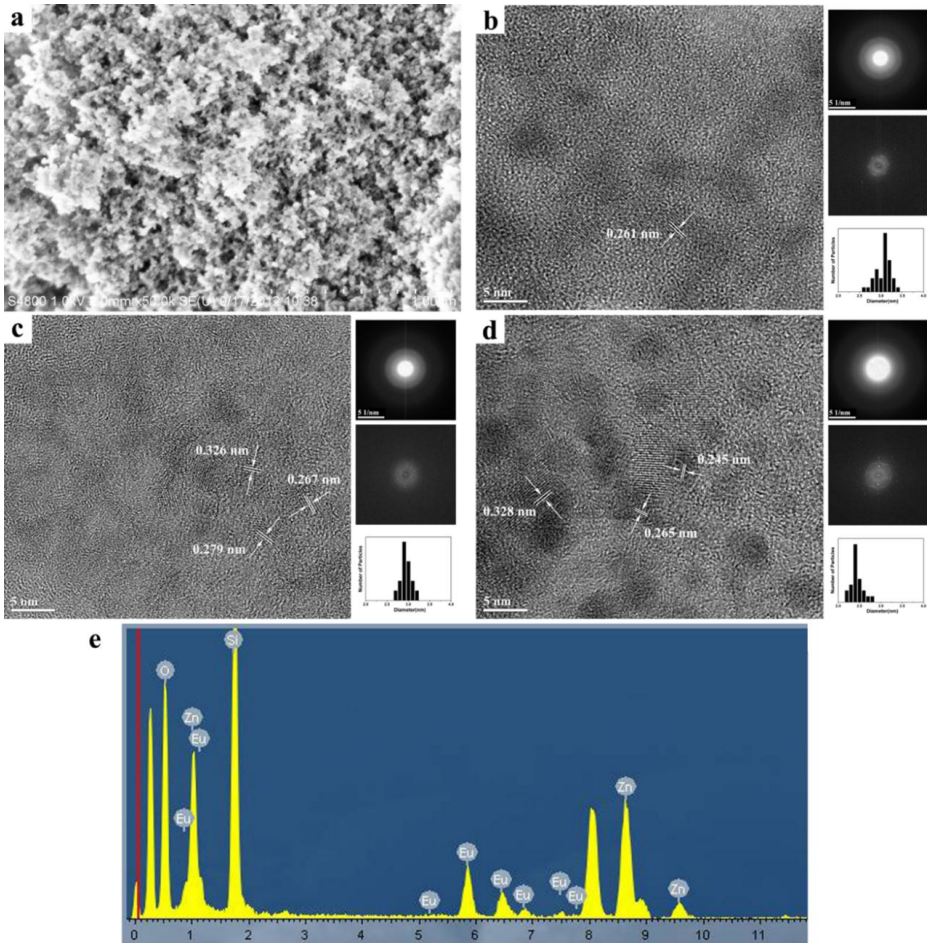

Figure 2. (a) SEM image of ZnO-Eu(5%)@SiO_2 annealed at 650 ^oC; (b-d) TEM images of the as-prepared ZnO-Eu(0%)@SiO_2, ZnO-Eu(5%)@SiO_2 and ZnO-Eu(20%)@SiO_2 samples, and the insets are the corresponding SAED pattern, FFT-HRTEM image and the size distribution of each sample; (e) A EDX spectrum obtained from the as-prepared ZnO-Eu(5%)@SiO_2 sample.

a result, the excess Eu species hider the growth of ZnO QDs, so as to decrease ZnO-Eu(m%) particle sizes [29]. The final Eu content in the SiO_2 matrix is generally lower than the added amount of Eu element in each reaction. The actual Eu/Zn ratios obtained from the ICP analyses are 0.0% (m = 0), 4.1% (m = 5), 7.4% (m = 10), 12.0% (m = 20) and 32.4% (m = 50), respectively. Besides the ICP results, the EDX spectrum also demonstrates the presence of Zn, Eu, O and Si elements in the final ZnO-Eu(m%)@SiO_2 (Figure 2e).

To investigate the chemical compositions and the binding states in ZnO-Eu(m%)@SiO_2, XPS measurements were performed and the results are analyzed in Figure 3. At first, the survey scan confirms the presence of Zn, O, Eu, Si and C elements. In the high-resolution scan of Zn $2p_3$, the double peaks at 1052.0 eV and 1028.8 eV are ascribed to the core levels of Zn $2p_{1/2}$ and Zn $2p_{3/2}$, respectively. When more and more Eu^{3+} ions are incorporated, the binding energy of the double peaks shift to the higher region gradually, which reconfirmed the Eu^{3+} ions have been doped in the ZnO lattice. In the asymmetric band of Eu 4d, two peaks at 148.0 eV and 144.6 eV are attributed to the core levels of Eu $4d_{3/2}$ and Eu $4d_{5/2}$, indicating the oxidation state of europium ions is trivalent for the doped ZnO QDs. The O1s band is asymmetric due to the existence of the crystal lattice oxygen and the chemisorbed oxygen. This band also shifts to high energy when Eu^{3+} ions are doped, which indicates that Eu(III) has formed chemical bonds with oxygen in the products.

The PL spectra of ZnO-Eu(m%)@SiO_2 samples before and after calcination are compared in Figure 4 a and c. When excited by UV light, all of the samples exhibit a broad green emission band of ZnO and a typical red emission peak of Eu^{3+} at 610 nm. It is interesting that the influences of Eu incorporation in ZnO QDs before and after calcination are just converse. Figure 4a shows the more Eu incorporation the higher the PL intensity of ZnO. In the meantime, both excitation curves and emission maxima of ZnO QDs blue-shift as more and more Eu^{3+} ions incorporate. Such phenomena are ascribed to the complex influences of Eu(III) species. On one hand, Eu(III) species inhibit ZnO QDs growth and render smaller ZnO QDs, in accord with the TEM results, so both excitation and emission spectra blue-shift obeying the quantum size effects. On the other, Eu(III) species produce more defects in ZnO QDs and thus enhance ZnO green emission which mainly arises from the oxygen defects on ZnO surfaces. This phenomenon also indicates that before calcination, Eu(III) species mainly locate on ZnO nanoparticle surfaces. On the contrary, Figure 4c shows the more Eu incorporation the lower the PL intensity of ZnO. In the meantime, both excitation curves and emission maxima of ZnO QDs do not shift but the PL intensity of Eu^{3+} ions increases gradually. Obviously, there is energy transfer from ZnO QDs to Eu^{3+} ions in the annealed ZnO-Eu(m%)@SiO_2 samples.

The efficiency of the fluorescence resonance energy transfer (FRET) can be calculated by a formula $E = 1 - F_{DA}/F_D$, where E is the efficiency, F_D is the original fluorescent

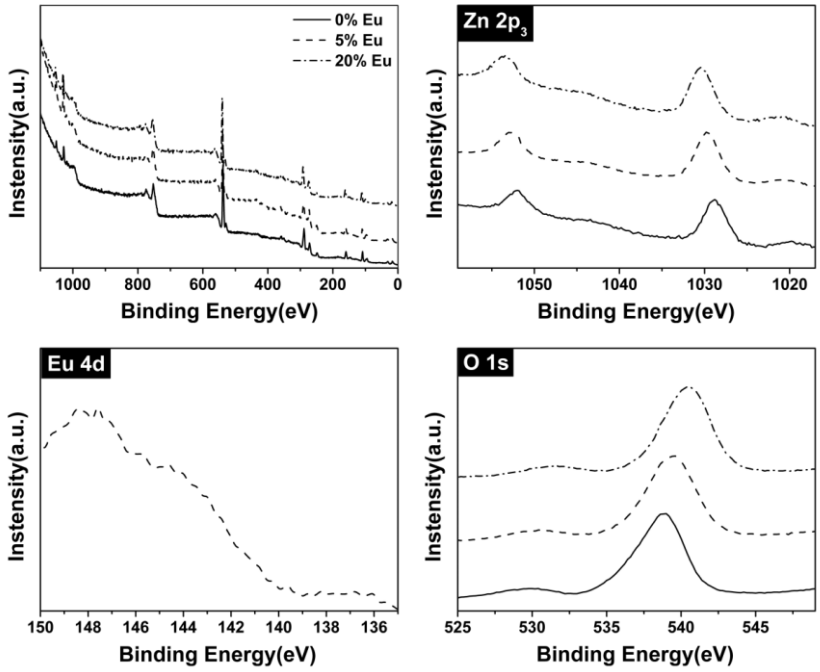

Figure 3. XPS spectra of ZnO-Eu(m%)@SiO_2 samples: survey scan, Zn 2p, Eu 4d and O1s signals.

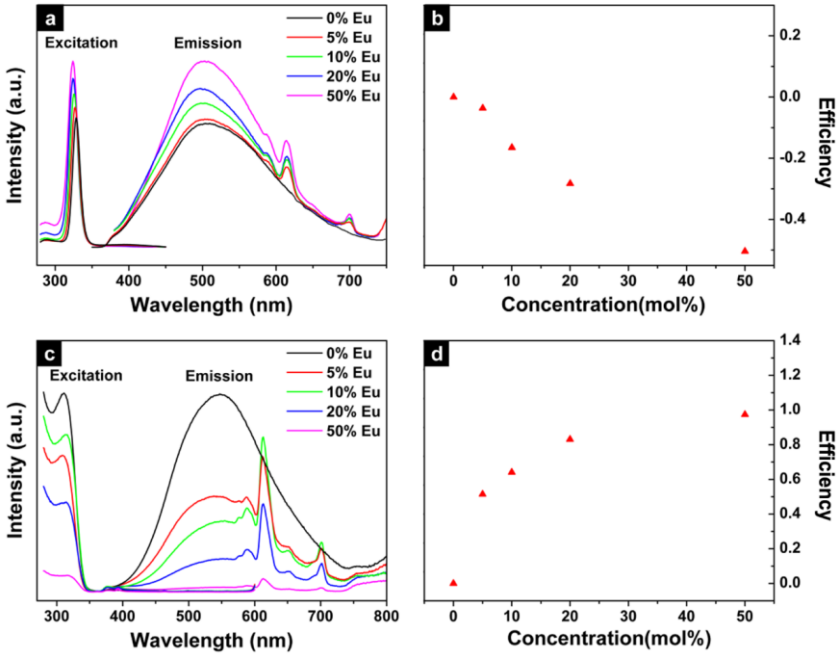

Figure 4. (a, c) PL spectra of ZnO-Eu(m%)@SiO_2 samples before and after calcination, respectively. (b, d) FRET efficiencies calculated according to the data in (a) and (c), respectively. The negative numbers of the calculated Efficiency in (b) confirms that there is no FRET in (a) actually.

intensity of the donor and F_{DA} is the fluorescent intensity of the donor after quenched by the acceptor. In Figure 4b, the efficiency value decreases gradually even below zero, hence actually there is no FRET in the ZnO-Eu(m%)@SiO_2 samples before calcination. But in Figure 4d, the efficiency value increases gradually from zero to about one, confirming that the FRET in the annealed ZnO-Eu(m%)@SiO_2 samples dominates the Eu(III) fluorescence. Although the ZnO-Eu(50%)@SiO_2 sample exhibits the highest FRET efficiency, the highest Eu(III) emission at 610 nm is observed in the ZnO-Eu(10%)@SiO_2 sample due to the concentration quenching effects, i. e., excess Eu^{3+} ions produce plenty of nonradiative defects and energy pathways so as to quench the energy from ZnO QDs. It should be mentioned that the enhanced Eu(III) fluorescence cannot be ascribed to the Eu_2O_3 nanoparticles in the SiO_2 matrix, because the ZnO-Eu(50%)@SiO_2 sample with the highest concentration of Eu_2O_3 nanoparticles exhibits the weakest fluorescence in Figure 4c.

In order to understand the FRET process in ZnO-Eu(m%)@SiO_2 samples deeply, the time-resolved transient fluorescent spectra were measured for three typical samples: m = 0, 5 and 20. The emission decay curves were fitted into a

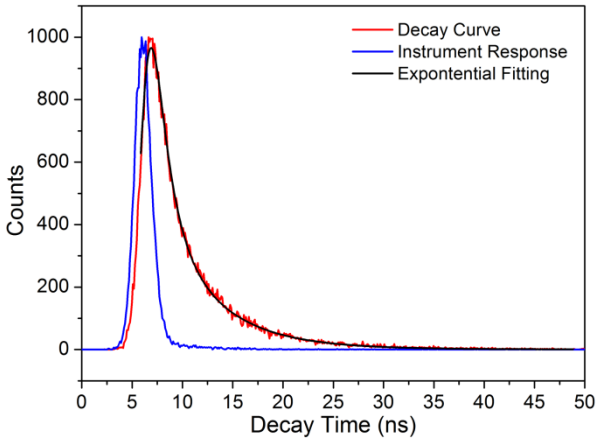

Figure 5. Time-resolved fluorescence decay curves of the annealed ZnO-Eu(5%)@SiO_2 samples. The decay curves of the other samples are similar.

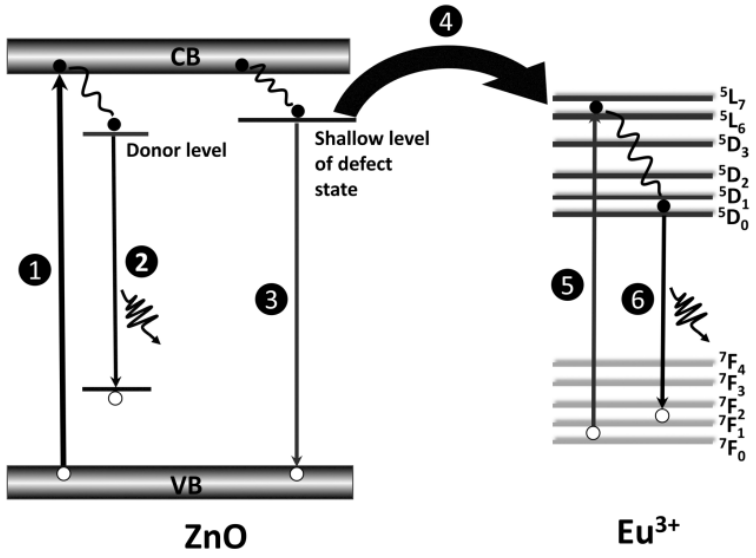

Scheme 1. The mechanisms for the luminescence and energy transfer in Eu^{3+}-doped ZnO QDs.

biexponential function $\tau = A_1 \exp(-t/\tau_1) + A_2 \exp(-t/\tau_2)$ and the average lifetime τ for these three samples are 3.94, 3.58 and 3.16 ns respectively. The excitation wavelength was 310 nm and the emission wavelength was detected at 540 nm, which were the features of ZnO visible fluorescence (Figure 5). Since the lifetime for ZnO visible emission is mainly controlled by the radiative recombination processes in the deeply trapped electrons and holes, more defect levels or deeper traps will delay the recombination time so as to extend the fluorescent lifetime. However, the decay curves show the more Eu^{3+} doping, the shorter the fluorescent lifetime, in accord with the decrease of ZnO visible emission. Therefore, when more and more Eu^{3+} ions are doped, more and more radiative recombination take place inside the Eu^{3+} dopants which have shorter lifetime of fluorescence. In the meantime, more defects are produced in the ZnO QDs, rending more nonradiative recombination and weaker PL emission overall. This speculation fits well with the results in our lifetime measurements.

On the basis of the above discussion, the luminescent mechanism of our ZnO-Eu(m%)@SiO_2 is illustrated in Scheme 1. Under UV light irradiation, photoelectrons are excited from the valence band (VB) to the conduction band (CB) (Process 1) of ZnO QDs, then relaxed to the donor levels (shallow traps) below CB, while the photo-generated holes are tunneled into accepter levels (deep traps) above VB. The recombination of shallowly trapped electrons and the deeply trapped holes (Process 2) is regard as the main mechanism for ZnO visible emission [30]. The shallowly trapped electrons can also jump down to VB and emit UV light of about 370 nm (Process 3), which is called exciton emission. This process has similar energy with the excitation transition (Process 5) of Eu^{3+}, and thus its energy can be transferred resonantly (Process 4) to the doped Eu^{3+} ions and finally render the typical $^5D_0$-^7F_J (J = 0~4) red emission (Process 6).

4. Conclusions

In summary, the Eu-doped ZnO QDs with effective energy transfer and red emission were successfully prepared via a sol-gel route and a calcination treatment. The SiO_2 matrix inhibited the aggregation and growth of ZnO QDs effectively, and in the meantime, the Eu^{3+} ions adsorbed on the ZnO grain surface diffused into the ZnO lattice during calcination. The

final ZnO-Eu(m%)@SiO_2 were dispersed in water and exhibited complex fluorescence which depends on m value critically. The highest red emission was observed when m = 10, while more Eu^{3+} incorporation quenched the visible emission of the whole sample. Based on the detailed optical measurements, a reasonable mechanism was put forward to illustrate the fluorescence emission and the fluorescence resonance energy transfer from ZnO to Eu^{3+} ions. The optimal sample exhibited stable red fluorescence in aqueous solution, which may find biological applications in the future.

Acknowledgements

This work was supported by the National Major Basic Research Program of China (2013CB934101), the National Natural Science Foundation of China (21271045), NCET-11-0115 and the Opening Fund of State Key Laboratory of Rare Earth Resource Utilization, Changchun Institute of Applied Chemistry, Chinese Academy of Sciences (RERU2013001).

References

1. P. Zhang, W. G. Liu, Biomaterials 31 (2010) 3087.
2. H. M. Xiong, Y. Xu, Q. G. Ren, Y. Y. Xia, J. Am. Chem. Soc. 130 (2008) 7522.
3. N. R. Jana, H. H. Yu, E. M. Ali, Y. G. Zheng, J. Y. Ying, Chem. Commun. 14 (2007) 1406.
4. W. H. Zhang, W. D. Zhang, J. F. Zhou, J. Mater. Sci. 45 (2010) 209.
5. Ü. Özgür, Ya. I. Alivov, C. Liu, A. Teke, M. A. Reshchikov, S. Do gan, V. Avrutin, S. J. Cho, H. Morkoc, J. Appl. Phys. 98 (2005) 041301.
6. A. P. Alivisatos, Science 271 (1996) 933.
7. Y. Yang, Y. Q. Li, S. Y. Fu, H. M. Xiao, J. Phys. Chem. C 112 (2008) 10553.
8. L. P. Liu, J. Hensel, R. C. Fitzmorris, Y. D. Li, J. Z. Zhang, J. Phys. Chem. Lett. 1 (2010) 155.
9. (a) X. Y. Zeng, J. L. Yuan, Zh. Y. Wang, L. D. Zhang, Adv. Mater. 19 (2007) 14510; (b) X. Y. Zeng, J. L. Yuan, L. D. Zhang, J. Phys. Chem. C 112 (2008) 3503.
10. L. Armelao, F. Heigl, A. Ju1rgensen, R. I. R. Blyth, T. Regier, X. T. Zhou, T. K. Sham, J. Phys. Chem. C 111 (2007) 10194.
11. L. Armelao, G. Bottaro, M. Pascolini, M. Sessolo, E. Tondello, M. Bettinelli, A. Speghini, J. Phys. Chem. C 112 (2008) 4049.
12. R. Chen, Y. Q. Shen, F. Xiao, B. Liu, G. G. Gurzadyan, Z. L. Dong, X. W. Sun, H. D. Sun, J. Phys. Chem. C 114 (2010) 18081.
13. D. D. Wang, G. Z. Xing, M. Gao, L. L. Yang, J. H. Yang, T. Wu, J. Phys. Chem. C 115 (2011) 22729.
14. Y. L. Yu, Y. S. Wang, D. Q. Chen, P. Huang, E. Ma, F. Bao, Nanotechnology 19 (2008) 055711.
15. M. Peres, A. Cruz, S. Pereira, M. R. Correia, M. J. Soares, A. Neves, M. C. Carmo, T. Monteiro, A. S. Pereira, M. A. Martins, T. Trindade, E. Alves, S. S. Nobre, R. A. Sá Feeeeira, Appl. Phys. A 88 (2007) 129.
16. A. Ishizumi, Y. Kanemitsu, Appl. Phys. Lett. 86 (2005) 253106.
17. Y. L. Liu, K. L. Ai, Q. H. Yuan, L. H. Lu, Biomaterials 32 (2011) 1185.
18. F. Xiao, R. Chen, Y. Q. Shen, Z. L. Dong, H. H. Wang, Q. Y. Zhang, H. D. Sun, J. Phys. Chem. C 116 (2012) 13458.
19. D. D. Wang, Q. Chen, G. Z. Xing, J. B. Yi, S. R. Bakaul, J. Ding, J. L. Wang, T. Wu, Nano Lett. 12 (2012) 3994.
20. L. W. Sun, H. Q. Shi, W. N. Li, H. M. Xiao, S. Y. Fu, X. Z. Cao, Z. X. Li, J. Mater. Chem. 22 (2012) 8221.
21. S. C. Erwin, L. Zu, M. I. Haftel, A. L. Efros, T. A. Kennedy, D. J. Norris, Nature 436 (2005) 91.
22. D. A. Chen, R. Viswanatha, G. L. Ong, R. G. Xie, M. Balasubramaninan, X. G. Peng, J. Am. Chem. Soc. 131 (2009) 9333.
23. R. S. Zeng, M. Rutherford, R. G. Xie, B. S. Zou, X. G. Peng, Chem. Mater. 22 (2010) 2107.
24. R. G. Xie, X. G. Peng, J. Am. Chem. Soc. 131 (2009) 10645.
25. R. Viswanatha, D. M. Battaglia, M. E. Curtis, T. D. Mishima, M. B. Johnson, X. G. Peng, Nano Res. 1 (2008) 138.
26. D. J. Norris, A. L. Efros, S. C. Erwin, Science 319 (2008) 1776.
27. Bachir S., Azuma K., Kossanyi J., Valat P., J. C. Ronfard-Haret, J. Lumin. 75 (1997) 35.
28. F. V. Mikulec, M. Kuno, M. Bennati, J. Am. Chem. Soc. 122 (2000) 2532.
29. Y. P. Du, Y. W. Zhang, L. D. Sun, C. H. Yan, J. Phys. Chem. C 112 (2008) 12234.
30. H. M. Xiong, J. Mater. Chem. 20 (2010) 4251.

Cite this article as:

Jue-Fei Zhou *et al.*: **Fluorescence resonance energy transfer within Eu(III)-doped ZnO quantum dots embedded in SiO_2 matrix.** Sci. Lett. 2015, **4**: 112